RSC Mechanochemistry

Accepted Manuscript

This article can be cited before page numbers have been issued, to do this please use: X. Liu, Y. Chen, Q. Ma, M. Yu, W. Guo, B. Wang, Q. Liu, R. Yu, Q. Liu and H. Liu, *RSC Mechanochem.*, 2026, DOI: 10.1039/D6MR00022C.

View Article Online
DOI: 10.1039/D6MR00022C

ARTICLE

Electromagnetic milling-promoted steel rods-enabled Sonogashira coupling reactions of aryl halides and terminal alkynes

Xinyao Liu,[a] Yanyan Chen,[a] Qiuhong Ma,[b,*] Meng Yu,[c] Wenjie Guo,[d] Baoju Wang,[a] Qiang Liu,[a] Rujun Yu,[a,*] Qing Liu[a,*] and Hui Liu[a,*]

Received 00th January 20xx,
Accepted 00th January 20xx

DOI: 10.1039/x0xx00000x

Nickel-catalyzed Sonogashira reactions between aryl halides and terminal alkynes have become a powerful method for constructing C(sp^2)–C(sp) bonds. Conventional approaches typically required copper co-catalysts, solvents, inert atmospheres, and external heating. Herein, we report an alternative and streamlined reductive C(sp^2)–C(sp) cross-coupling protocol that employs inexpensive nickel catalyst, eliminating the need for Ni/Cu dual catalysts. This electromagnetic milling (EMM) promoted strategy effectively circumvents the constraints associated with traditional nickel-catalyzed Sonogashira reactions. Mechanistic studies reveal that Ni(II) precursor in $NiCl_2$ is activated under magnetic field and in the presence of DABCO to produce Ni(0) as the active catalyst, and EMM plays a critical role in promoting reductive elimination from Ni^{II} complex.

Introduction

As versatile building blocks in organic chemistry, alkynes are widely used in fields from biochemistry to materials science and drug discovery. [1-9] Consequently, significant efforts are focused on developing efficient methods to incorporate alkyne moieties into molecules for synthesizing substituted internal alkynes. The Sonogashira reaction is widely regarded as the leading C–C(sp) cross-coupling method, traditionally pairing terminal alkynes and electrophiles using a palladium catalyst with or without a copper co-catalyst (Figure 1A).[10-15] Additionally, recent research has focused on developing Sonogashira-type reactions using precious transition metals like Co, Ir and Rh, as alternatives to traditional palladium catalysts.[16-22] Meanwhile, nickel catalysts, as low toxic and ready commercially available transition metals, attracted great interest in the development of Sonogashira reactions.[23,24] However, most existing nickel-catalyzed Sonogashira cross-coupling reactions of aryl halides with terminal alkynes still depend on copper co-catalysts (Figure 1B). In the solution phase, Liao's team achieved nickel-catalyzed Sonogashira coupling without copper co-catalysts, albeit requiring 48 hours of reaction time in DMAc solvent at 60 °C (Figure 1C). [26]

Mechanochemistry, as a representative technology in green synthesis, enables efficient homogenization of reactants through mechanical energy input, significantly reducing or eliminating the use of organic solvents.[27-43] However, Sonogashira reactions under mechanochemical conditions have predominantly relied on palladium catalysts[44-47] or noble metal alloys (e.g., Pd-Ni). In 2024, the Borchardt research group reported the first instance of mechanocatalytic Sonogashira reactions using a Pd–Ni alloy containing 20% palladium in a ball mill, achieving over 80% yield within one hour under solvent-free conditions without external heating.[48] In summary, to date, a mechanochemical Sonogashira reaction using a pure nickel catalyst without copper co-catalysts under solvent-free and externally unheated conditions has not been reported.

As an innovative milling device, the electromagnetic mill (EMM) employs ferromagnetic particles as the milling medium, utilizing an axially rotating electromagnetic field to drive ferromagnetic rods at high speed, achieving efficient mixing and energy transfer of solid reactants while offering advantages such as high energy efficiency and excellent controllability.[49-51] Our previous research has successfully applied electromagnetic milling technology to organic synthesis, achieving palladium/copper dual-catalyzed Sonogashira cross-coupling reactions under solvent-free and externally unheated conditions. [52] Building on this foundation, this paper reports a Sonogashira cross-coupling reaction utilizing pure nickel catalysis under EMM conditions, achieved without solvent, external heating, or copper co-catalysts, thereby providing a

[a] School of Chemistry and Chemical Engineering, Shandong University of Technology Zibo, Shandong 255049, China
[b] Department of Clinical Laboratory, Zibo Central Hospital affiliated to Binzhou Medical University, Shandong 255049, China
[c] Zibo Construction Project Environmental Review Service Center, Shandong 255049, China
[d] Shandong Diam Chemical Co., Ltd, Shandong 256800, China

more environmentally friendly and sustainable strategy for constructing C(sp)-C(sp²) bonds.

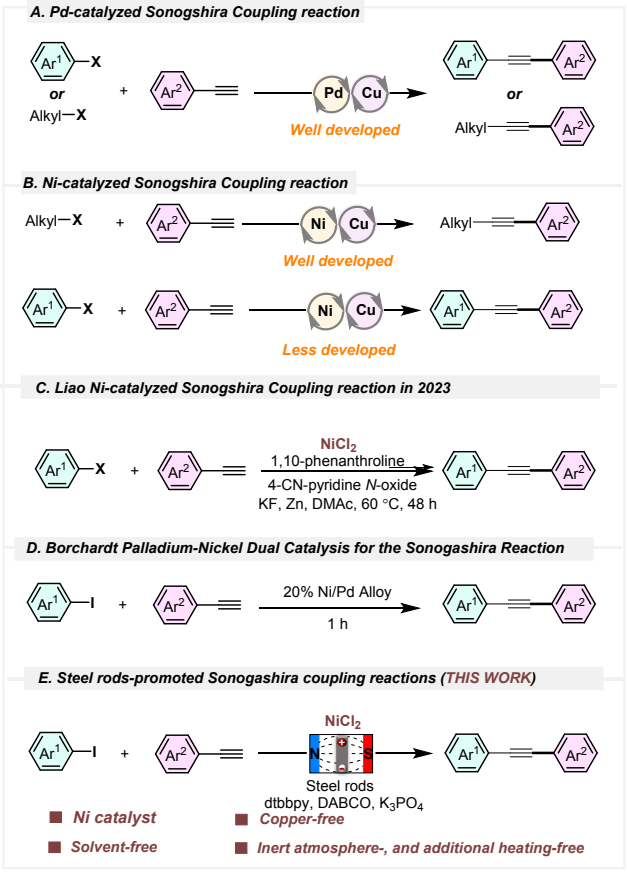

Figure 1. The development of Sonogashira reaction.

Results and Discussion

The research commenced by exploring the reaction between p-terbutyliodobenzene **1a** and phenylacetylene **2a** in the presence of [$NiCl_2(PPh_3)_2$], 1,4-diazahecyclic [2.2.2] octane (DABCO), K_3PO_4, 4,4'-di-tert-butyl-2,2'-bipyridine (dtbbpy) and steel rods using EMM at a frequency of 50 Hz, which afforded the desired product **3a** in 83% yield (Table 1, entry 1). Several nickel catalysts were initially examined, including nickel powder, $NiBr_2$, $NiCl_2$, Ni(dppf)$_2$ and Ni(COD)$_2$. Among these, the reaction with $NiCl_2$ exhibited the best performance, achieving a 90% yield (Table 1, entries 2–6). Further investigation of the reaction components showed that the absence of the ligand dtbbpy resulted in a reduced yield (entry 7), while the elimination of DABCO or K_3PO_4 led to almost no reaction (entries 8–10). Based on these findings, the influence of various ligands and bases was explored, and it was determined that dtbbpy and K_3PO_4 were the optimal choices (entries 11–17). When DABCO was replaced with Et_3N and DBU, the reaction yields decreased to 80% and 85%, respectively (entries 18 and 19). In contrast, the strongly reducing nature of Zn powder led to preferential reduction of the alkyne to the alkane, rendering the coupling reaction nearly inoperative and resulting in a substantial decrease in the reaction yield (entry 20). The optimal conditions for the reaction were using $NiCl_2$ as the catalyst, dtbbpy as the ligand, K_3PO_4 as the base, DABCO as the additive, and steel rods under EMM at 50 Hz.

Table 1. Optimization of Conditions[a].

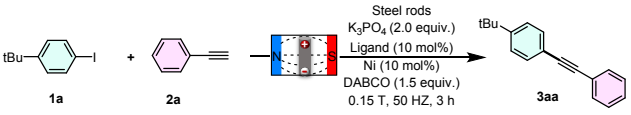

Entry	Ni	Additive	Base	Ligand	Rods	Yield(%)
1	$NiCl_2(PPh_3)_2$	DABCO	K_3PO_4	L_1	steel rods	83%
2	Ni powder	DABCO	K_3PO_4	L_1	steel rods	15%
3	$NiBr_2$	DABCO	K_3PO_4	L_1	steel rods	85%
4	$NiCl_2$	DABCO	K_3PO_4	L_1	steel rods	90%
5	$Ni(dppf)Cl_2$	DABCO	K_3PO_4	L_1	Steel rods	84%
6	$Ni(COD)_2$	DABCO	K_3PO_4	L_1	Steel rods	75%
7	$NiCl_2$	DABCO	K_3PO_4	\	steel rods	12%
8	$NiCl_2$	\	K_3PO_4	\	steel rods	ND
9	$NiCl_2$	\	K_3PO_4	L_1	steel rods	ND
10	$NiCl_2$	DABCO	\	L_1	steel rods	ND
11	$NiCl_2$	DABCO	K_3PO_4	L_2	steel rods	60%
12	$NiCl_2$	DABCO	K_3PO_4	L_3	steel rods	74%
13	$NiCl_2$	DABCO	K_3PO_4	L_4	steel rods	75%
14	$NiCl_2$	DABCO	K_3PO_4	L_5	steel rods	76%
15	$NiCl_2$	DABCO	K_2CO_3	L_1	steel rods	73%
16	$NiCl_2$	DABCO	Na_2CO_3	L_1	steel rods	79%
17	$NiCl_2$	DABCO	Cs_2CO_3	L_1	steel rods	85%
18	$NiCl_2$	Et_3N	K_3PO_4	L_1	steel rods	80%
19	$NiCl_2$	DBU	K_3PO_4	L_1	steel rods	85%
20	$NiCl_2$	Zn powder	K_3PO_4	L_1	steel rods	33%

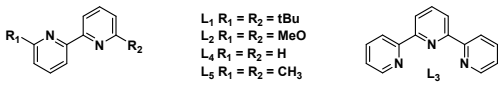

Conditions: [a] **1a** (0.6 mmol, 2 equiv.), **2a** (0.3 mmol, 1 equiv.), Catalyst (10 mol%), Ligand (10 mol%), DABCO (1.5 equiv.), K_3PO_4 (2.0 equiv.), steel rods (0.3 mm×5.0 mm, 5 g), 0.15 T, 50 Hz, 3 h.

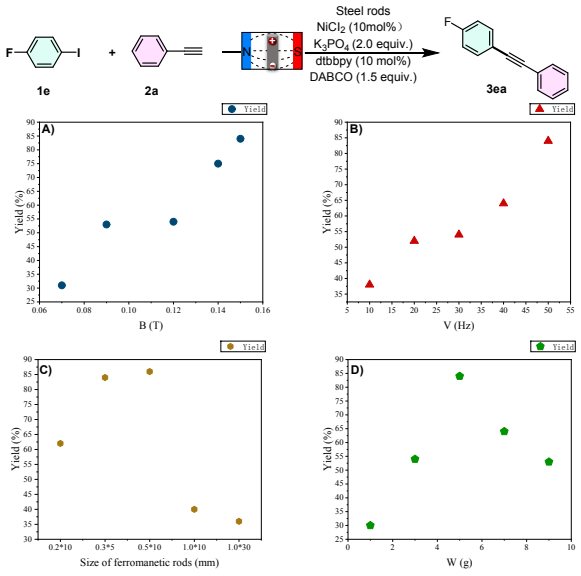

Figure 2. Optimization of parameters in EMM. Conditions: A) Effect of magnetici-ntensity on reaction (5g, size of steel rods is 0.3*5 mm, v = 50 Hz). B) Effect of rotating frequency on the reaction (B = 0.15 T, 5g, size of rods is 0.3*5 mm). C) Effect of size of steel rods on the reaction (5g, B = 0.15 T, v = 50 Hz). D) Effect of weight of steel rods on the reaction (B = 0.15 T, v = 50 Hz, size of rods is 0.3*5 mm).

After determining the initial reaction conditions, the equipment parameters were further optimized (Figure 2). The magnetic field strength was adjusted (0.07–0.15 T) by changing the position of the reaction tube, leading to a proportional increase in reaction efficiency (Figure 2A). Increasing the frequency from 10 to 50 Hz also enhanced the yields (Figure 2B). Screening of the ferromagnetic rods identified a diameter of 0.3 mm and a length of 5 mm as optimal, likely due to their ability to maximize collision speed and intensity (Figure 2C). Finally, a loading mass of 5 g was found to be optimal, as other amounts caused non-uniform agitation (Figure 2D).

Table 2. Substrate scope.

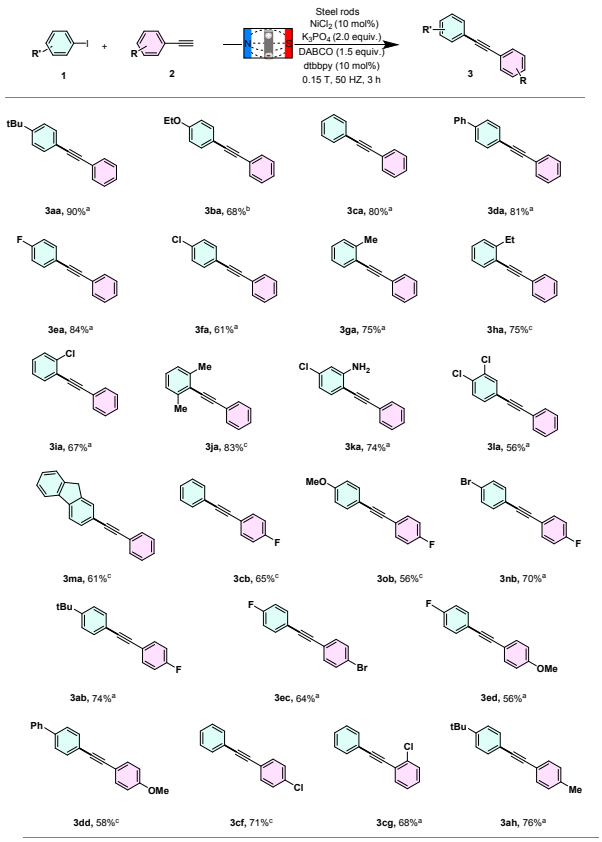

Reaction conditions: [a] **1** (0.6 mmol, 2 equiv.), **2** (0.3 mmol, 1 equiv.), $NiCl_2$ (10 mol%), dtbbpy (10 mol%), DABCO (0.45 mmol ,1.5 equiv.), K_3PO_4 (0.6 mmol, 2 equiv.), steel rods (0.3 mm×5.0 mm, 5 g), 0.15 T, 50 Hz, 3 h. [b] **1** (0.3 mmol, 1 equiv.), **2** (0.6 mmol, 2 equiv.). [c] **1** (0.3 mmol, 1 equiv.), **2** (0.3 mmol, 1 equiv.)

With the optimal conditions established, the substrate scope of the coupling reactions was explored (Table 2). Both electron-donating (tBu, OEt, and H) and electron-withdrawing (Ph, F, and Cl) groups at the para position of aryl iodides were tolerated, resulting in the desired products **3aa-3fa** in moderate to high yields. Ortho-substituted groups (2-Me, 2-Et and 2-Cl) were also tolerated, yielding products **3ga-3ia**. Disubstituted substrates at the para- and meta- or ortho-positions of the benzene ring of aryl iodides also afforded the desired products (**3ja-3la**). Notably, 2-iodofluorene was successfully coupled, providing the desired product **3ma** in 61% yield. The scope of arylacetylene substrates was also investigated. Under the optimized reaction conditions, both electron-donating (4-OMe and 4-Me) and electron-withdrawing (4-F, 4-Cl, 2-Cl, and 4-Br) substituted arylacetylenes reacted smoothly with various functionalized aromatic iodides, such as iodobenzene, 4-tert-butyl iodobenzene, and 4-fluoroiodobenzene, affording the corresponding products in acceptable yields (**3cb–3ah**). Poorly soluble substrate polyaryl halide (1-iodobiphenyl) underwent reactions with phenylacetylene and p-methoxyphenylacetylene, respectively, affording the target products in excellent yields (**3da**, 81% and **3dd**, 58%). Additionally, bromobenzene was also examined in the standard conditions with phenylacetylene, giving the coupling product **3ca** in 20% yield.

Elemental analysis confirmed the presence of key metallic elements (i.e., Fe, Ni, Cr) in the steel rods. To elucidate the reaction mechanism and determine the origin of the catalytically active nickel, a series of mechanistic and control experiments were conducted (Figure 3). Initially, the reaction was carried out using Fe rods instead of steel rods, in the absence of externally added $NiCl_2$. No desired product **3ab** was detected, confirming that the coupling reaction could not proceed under these conditions (Figure 3A). Consequently, Fe rods were used to replace steel rods in all subsequent experiments to eliminate potential interference from other elements in the steel.

Subsequently, different loadings of nickel salts ($NiCl_2(PPh_3)_2$, $NiCl_2$, and $NiBr_2$) were individually combined with Fe rods for the reaction. The results showed that all three nickel salts effectively facilitated the formation of the desired product, with the yield progressively increasing as the dosage of the nickel catalyst was raised (Figure 3B). Notably, $NiCl_2$ delivered the highest yield among the tested salts, suggesting its superior catalytic efficiency under identical conditions. The linear correlation between catalyst loading and product yield further supports a well-defined catalytic cycle rather than stoichiometric participation. Additionally, control experiments without nickel salts afforded no detectable product, underscoring the indispensable role of the nickel species in enabling this transformation.

To further rule out the contribution of nickel derived from the steel rods, the steel rods were directly milled under EMM coupling conditions, and the resulting trace powder was introduced into the model reaction. No target product 3ab was detected in this case. Meanwhile, control experiments using Ni rods alone or Fe rods combined with Ni powder also failed to yield the desired product (Figure 3C). Additionally, to exclude any possible synergistic effect between nickel (released from milled steel rods) and Fe/Cr, combined reactions of Ni rods with

View Article Online
DOI: 10.1039/D5MR00023G

Fe powder and Cr powder were carried out, but no target product was obtained either (Figure 3D).

To elucidate the role of DABCO in the reaction, three sets of control experiments were conducted (Figure 3E). Using $NiCl_2$ as the Ni(II) source with 1.5 equiv. of DABCO delivered the desired product in 74% yield. However, no reaction was detected in the absence of DABCO. These results indicated that Ni(II) could not initiate the coupling reaction, but DABCO could convert it to the active nickle species. Furthermore, using $Ni(COD)_2$ as the Ni(0) source could produce the corresponding product in 32% yield, establishing the intrinsic activity benchmark for Ni(0) catalysts in this system. The addition of 10% of DABCO increased the yield to 38%, demonstrating that DABCO might play an important role in the nickle catalysis cycle. Collectively, these findings unambiguously establish that nickel released from milled steel rods is catalytically inactive in the reaction system, and NiCl2 serves as the true catalytic component for the Sonogashira coupling reaction.

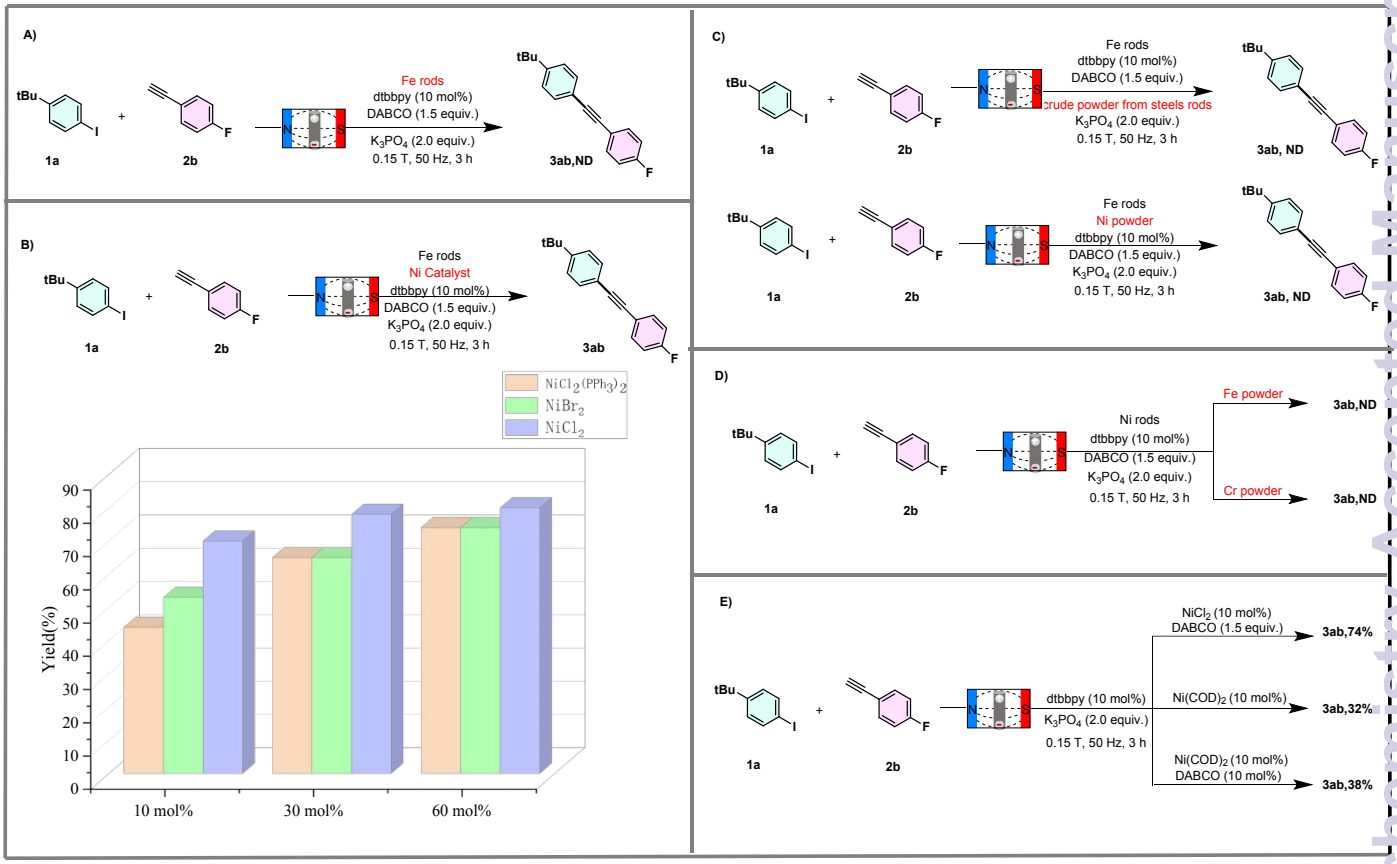

Figure 3. Mechanistic investigation. Conditions: **1a** (0.6 mmol, 2 equiv.), **2b** (0.3 mmol, 1 equiv.), dtbbpy (10 mol%), DABCO (1.5 equiv.), K_3PO_4 (2.0 equiv.), Fe rods (1.0 mm×5.0 mm, 5 g), Ni rods (1.0 mm×5.0 mm, 5 g), 0.15 T, 50 Hz, 3 h.

Based on the XPS analysis results (Figure 4), the following summary can be made: In the reference spectrum of $NiCl_2$, the Ni $2p_{3}/_{2}$ peak exhibits a distinct Ni^{2+} main peak (~855 eV) accompanied by its characteristic satellite peaks, consistent with an octahedral coordination environment, indicating that nickel exists in a stable divalent state (Figure 4A). In complex **1**, the Ni^{2+} signal intensity is significantly diminished, with the main peak and satellite peaks nearly submerged by noise, suggesting that under the combined action of mechanical grinding and DABCO, Ni^{2+} is reduced to a low-valent Ni^{0} species. Owing to the high electron cloud density and enhanced shielding effect of Ni^{0}, the XPS signal intensity is substantially reduced and the peak shape is broadened, marking the successful generation of the catalytically active zero-valent nickel species (Figure 4B). In contrast, the spectrum of the sample subjected only to stirring closely resembles that of pure $NiCl_2$, retaining strong and well-defined Ni^{2+} characteristic signals with only minor changes in peak shape (Figure 4C), indicating that dtbbpy and DABCO couldn't reduce Ni^{2+} without mechanical grinding. Furthermore, the mixture of Ni and dtbbpy subjected to mechanical grinding in the absence of DABCO, showing no evidence of reduction (Figure 4D). These results demonstrate that DABCO is the key reductant enabling the $Ni^{2+} \rightarrow Ni^{0}$ transformation, and its reducing capability is dependent on the energy input provided by mechanical grinding.

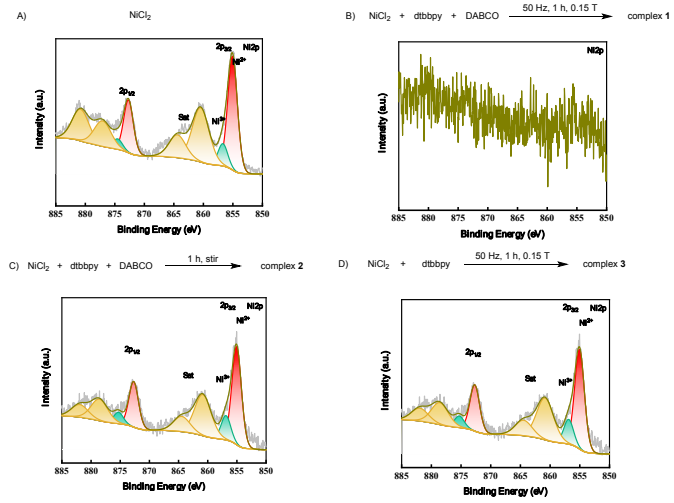

Figure 4. XPS spectra elucidating the roles of DABCO and mechanical grinding in the nickel reduction process.

To assess the practicality and scale-up potential, the reaction was conducted on a 2 mmol scale for gram-scale synthesis (Figure 5). The transformation proceeded smoothly, delivering the target product **3aa** in 80% yield (0.37 g), thereby establishing a foundation for its potential industrial application.

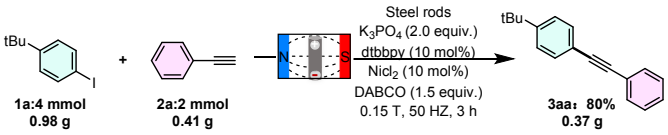

Figure 5. Gram-scale reaction.

Based on the combination of above experiments and reported literatures, a plausible catalytic cycle was delineated in Figure 6. Ni(II) in $NiCl_2$ is reduced under magnetic field and in the presence of DABCO, forming a Ni^0L_2 complex with the ligand dtbbpy. Subsequently, the oxidative addition of [dtbbpyNi^0] (**4**) with aryl iodides gave aryl-Ni(II)-iodide complex **5**. The coordination and subsequent transfer of alkyne to **5** yielded intermediate **6** in the presence of K_3PO_4 and DABCO. Finally, reductive elimination resulted in the formation of the target product **3** and the regeneration of the Ni^0 catalyst under magnetic field. Generally, reductive elimination from a Ni(II) complex is a thermodynamically unfavorable process. In this strategy, the promoted reductive elimination from complex **6** may be attributed to the magnetic field.

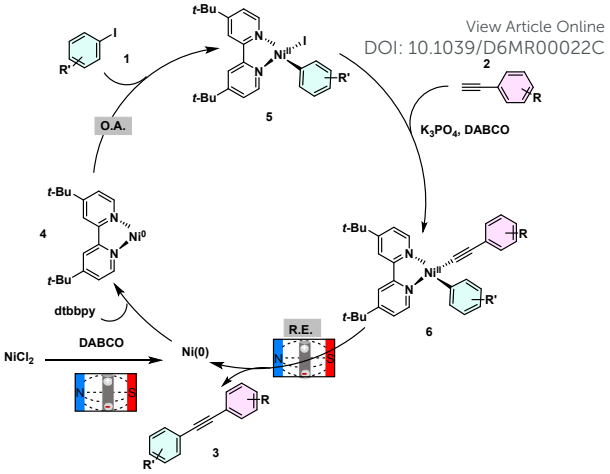

Figure 6. Proposed mechanism.

Conclusions

In summary, an electromagnetic mill-promoted Sonogashira coupling reaction of aryl halides and terminal alkynes was developed, utilizing $NiCl_2$ as the nickel catalyst source. This method demonstrated significant advantages by eliminating the need for additional precious transition metal catalysts, solvents, inert-gas atmospheres, and external heating. The easily operable methodology also showed excellent tolerance for various substitutions and a wide substrate scope. Mechanistic investigations revealed that the Ni(II) precursor in $NiCl_2$ is activated to form a Ni(0) catalyst under the influence of the magnetic field and DABCO, facilitating the coupling reaction. The electromagnetic milling enhances the transfer of alkynes to the Ni(II) species. This strategy is expected to provide a viable alternative for alkyne synthesis.

Author contributions

All authors have reviewed the manuscript.

Conflicts of interest

There are no conflicts to declare.

Data availability

Supplementary information (SI): all supporting experimental data, including copies of ^{1}H, ^{19}F and ^{13}C NMR spectra.

References

1 K. C. Nicolaou, C. W. Hummel, E. N. Pitsinos, M. Nakada, A. L. Smith, K. Shibayama and H. Saimoto, *J. Am. Chem. Soc*., 1992, **114**, 10082–10084.
2 J. Taunton, J. L. Wood and S. L. Schreiber, *J. Am. Chem. Soc*., 1993, **115**, 10378–10379.

3 Y. Koyama, M. J. Lear, F. Yoshimura, I. Ohashi, T. Mashimo and M. Hirama, *Org. Lett*., 2005, **7**, 267–270.
4 I. Paterson and T. Paquet, *Org. Lett*., 2010, **12**, 2158–2161.
5 R. Chinchilla and C. Nájera, *Chem. Soc. Rev*., 2011, **40**, 5084–5121.
6 B. De Carné-Carnavalet, A. Archambeau, C. Meyer, J. Cossy, B. Folléas, J. L. Brayer and J. P. Demoute, *Chem. Eur. J*., 2012, **18**, 16716–16727.
7 B. Vaz, L. Otero, R. Álvarez and Á. R. de Lera, *Chem. Eur. J*., 2013, **19**, 13065–13074.
8 M. Esmaeilpour, A. Sardarian and J. Javidi, *Catal. Sci. Technol*., 2016, **6**, 4005–4019.
9 J. S. Cyniak, Ł. Kocobolska, N. Bojdecka, A. Gajda-Walczak, A. Kowalczyk, B. Wagner, A. Nowicka, H. Sakurai and A. Kasprzak, *Dalton Trans*., 2023, **52**, 3137.
10 K. Sonogashira, Y. Tohda and N. Hagihara, *Tetrahedron Lett*., 1975, **16**, 4467–4470.
11 M. S. M. Ahmed and A. Mori, *Org. Lett*., 2003, **5**, 3057.
12 T. Lauterbach, M. Livendahl, A. Rosellón, P. Espinet and A. M. Echavarren, *Org. Lett*., 2010, **12**, 3006–3009.
13 M. Trunk, A. Herrmann, H. Bildirir, A. Yassin, J. Schmidt and A. Thomas, *Chem. Eur*. J., 2016, **22**, 7179–7183.
14 D. D. Vo and M. Elofsson, *ChemistrySelect*, 2017, **2**, 6245–6248.
15 H. Yanık, S. Yesilot and M. Durmus, *Dyes Pigm*., 2017, **140**, 157–165.
16 C. M. R. Volla and P. Vogel, *Tetrahedron Lett*., 2008, **49**, 5961–5964.
17 M. Carril, A. Correa and C. Bolm, *Angew. Chem. Int. Ed*., 2008, **47**, 4862–4865.
18 H. Huang, H. Jiang, K. Chen and H. Liu, *J. Org. Chem*., 2008, **73**, 9061–9064.
19 M. Karak, L. C. A. Barbosa and G. C. Hargaden, *RSC Adv*., 2014, **4**, 53442–53466.
20 L. Jin, W. F. Hao, J. N. Xu, N. Sun, B. X. Hu, Z. Shen, W. Mo and X. Hu, *Chem. Commun*., 2017, **53**, 4124–4127.
21 A. Hazra, M. T. Lee, J. F. Chiu and G. Lalic, *Angew. Chem. Int. Ed*., 2018, **57**, 5492–5496.
22 J. Y. Song, X. Zhou, H. Song, Y. Liu, H. Y. Zhao, Z. Z. Sun and W. Y. Chu, *ChemCatChem*, 2018, **10**, 758–762.
23 D. Gallego, A. Brueck, E. Irran, F. Meier, M. Kaupp, M.Driess and J. F. Hartwig, *J. Am. Chem. Soc.*, 2013, **135**, 15617-15626.
24 N. Hussain, P. Gogoi, P. Khare and M. R. Das, *RSC Adv*., 2015, **5**, 103105–103115.
25 D. L. Zhu, R. J. Xu, Q. Wu, H. Y. Li, J. P. Lang and H. X. Li, *J. Org. Chem.*, 2020, **85**, 12457–12465.
26 H. Chen, L. Yao, L. Guo, Y. A. Liu, B. Tian and X. Liao, *Cell Rep. Phys. Sci*., 2023, **4**, 101573.
27 G.-W Wang, *Chem. Soc. Rev*., 2013, **42**, 7668–7700.
28 K. Kubota, Y. Pang, A. Miura and H. Ito*, Science*, **2019**, 366, 1500–1504.
29 J. Zhang, P. Zhang, L. Shao, R. H. Wang, Y. Ma and M. Szostak, *Angew. Chem. Int. Ed*., 2022, **61**, e202114146.
30 R. R. A. Bolt, S. E. Raby-Buck, K. Ingram, J. A. Leitch and D. Browne, *Angew. Chem. Int. Ed*., 2022, **61**, e202210508.
31 X. Yang, C. Wu, W. Su and J. Yu, *Eur. J. Org. Chem*., 2022, **6**, e202101440.
32 X. Yang, H. Wang, Y. Zhang, W. Su and J. Yu, *Green Chem.*, 2022, **24**, 4108–4116.
33 C. Wu, T. Ying, H. Fan, C. Hu, W. Su and J. Yu, *Org. Lett.*, 2023, **25**, 2531–2536.
34 A. R. R. Hernandez, I. Trakakis, J. Cuccia and T. Friščić, *Eur. J. Org. Chem*., 2023, **26**, e202300374.
35 T. Seo, K. Kubota and H. Ito, *J. Am. Chem. Soc*., 2023, **145**, 6823–6837.
36 C. Patel, E. André-Joyaux, J. Leitch, X. Irujo-Labalde, F. Ibba, J. Struijs, M. Ellwanger, R. Paton, D. Browne, G. Pupo, S. Aldridge, M. Hayward and V. Gouverneur, *Science*, 2023, **381**, 302–306.
37 S. Pan, F. F. Mulks, P. Wu, K. Rissanen and C. Bolm, *Angew. Chem. Int. Ed*., 2024, **63**, e202316702.
38 X. Wang, X. Zhang, X. He, G. Guo, Q. Huang, F. Q. Wang, R. Qu, F. Zhou and Z. Lian, *Angew. Chem. Int. Ed*., 2024, **63,** e202410334.
39 R. Qu, S. Wan, X. Zhang, X. Wang, L. Xue, Q. Wang, G. Cheng, L. Dai and Z. Lian, *Angew. Chem. Int. Ed*., 2024, **63**, e202400645.
40 H. Lei, B. Wang, Y. Yang, S. Fan, S. Wang and X. Wei, *Org. Lett*., 2024, **26**, 7688–7694.
41 M. Hribersek, C. Méndez-Gálvez, M. Huber, P. Gates, P. Shakari, A. Samanta and L. Pilarski, *Green Chem*., 2023, **25**, 9138–9145.
42 S. Hutsch, A. Leonard, S. Graetz, M. Höfler, T. Gutmann and L. Borchardt, *Angew. Chem. Int. Ed*., 2024, **63**, e202403649.
43 V. Chantrain, T. Rensch, W. Pickhardt, S. Grätz and L. Borchardt, *Chem. Eur. J.*, 2024, **30**, e202304060.
44 D. A. Fulmer, W. C. Shearouse, S. T. Mendonza and J. Mack, *Green Chem*., 2009, **11**, 1821.
45 R. Thorwirth, A. Stolle and B. Ondruschka, *Green Chem*., 2010, **12**, 985.
46 Y. Gao, C. Feng, T. Seo, K. Kubota and H. Ito, *Chem. Sci*., 2022, **13**, 430–438.
47 W. Pickhardt, E. Siegfried, S. Fabig, M. F. Rappen, M. Etter, M. Wohlgemuth, S. Grätz and L. Borchardt, *Angew. Chem. Int. Ed*., 2023, **62**, e202301490.
48 W. Pickhardt, F. J. L. Kraus, M. Wohlgemuth, M. Etter, M. Spallek, M. Schwensow, Z. Genç, S. Grätz and L. Borchardt, ChemCatChem, 2024, **16**, e202400491 (1 of 5).
49 M. Wołosiewicz-Głąb, S. Ogonowski and D. Foszcz, *IFAC-PapersOnLine*, 2016, **49**, 67.
50 M. Wołosiewicz-Głąb, D. Foszcz and S. Ogonowski, *IFAC-PapersOnLine*, 2017, **50**, 14964.
51 M. Pawelczyk, Z. Ogonowski, S. Ogonowski, D. Foszcz, D. Saramak, T. Gawenda and D. Krawczykowski, *Minerals*, 2018, **8**, 138.
52 X. Zhang, Q. Liu, J. Gao, L. Zhang, F. Yan, S. Zhou and H. Liu, *Adv. Synth. Catal*., 2025, **367**, e202500100.

View Article Online
DOI: 10.1039/D6MR00022C

Data Availability Statement

Supplementary information (SI): all supporting experimental data, including copies of ^{1}H, ^{19}F and ^{13}C NMR spectra.